An energetics study of wintertime Northern Hemisphere storm tracks under 4 x CO_2 conditions in two ocean–atmosphere coupled models

Alexandre Laine, Masa Kageyama, David Salas-Mélia, Gilles Ramstein, Serge Planton, Sébastien Denvil, Sophie Tyteca

An Energetics Study of Wintertime Northern Hemisphere Storm Tracks under $4 \times CO_2$ Conditions in Two Ocean–Atmosphere Coupled Models

ALEXANDRE LAÎNÉ AND MASA KAGEYAMA

LSCE/IPSL, UMR CEA-CNRS-UVSQ, Saclay, Gif-sur-Yvette, France

DAVID SALAS-MÉLIA

CNRM/GAME, Météo-France/CNRS, Toulouse, France

GILLES RAMSTEIN

LSCE/IPSL, UMR CEA-CNRS-UVSQ, Saclay, Gif-sur-Yvette, France

SERGE PLANTON

CNRM/GAME, Météo-France/CNRS, Toulouse, France

SÉBASTIEN DENVIL

LMD/IPSL, CNRS-Université Paris VI, Paris, France

SOPHIE TYTECA

CNRM/GAME, Météo-France/CNRS, Toulouse, France

(Manuscript received 4 September 2007, in final form 20 June 2008)

ABSTRACT

Different possible behaviors of winter Northern Hemisphere storm tracks under $4 \times CO_2$ forcing are considered by analyzing the response of two of the ocean–atmosphere coupled models that were run for the fourth Assessment Report of the Intergovernmental Panel on Climate Change (IPCC-AR4), namely the Institut Pierre Simon Laplace's global coupled model (IPSL-CM4) and the Centre National de Recherches Meteorologiques's coupled ocean–atmosphere model (CNRM-CM3). It is interesting to compare these models due to their very different responses, especially concerning the North Atlantic storm track.

A local energetics study of the synoptic variability in both models is performed, derived from the eddy energy equations, including diabatic terms. The ability of both models to simulate the present-day eddy energetics is considered, indicating no major discrepancies.

Both models indicate that the primary cause for synoptic activity changes at the western end of the storm tracks is related to the baroclinic conversion process, due to mean temperature gradient changes in some localized regions of the western oceanic basins, but also resulting from changes in the eddy efficiency to convert energy from the mean flow. Farther downstream, latent heat release during the developing and mature stages of eddies becomes an important eddy energy source especially in terms of changes between $4 \times CO_2$ and preindustrial conditions. This diabatic process amplifies the upstream synoptic (hence usually baroclinic) changes, with more and/or stronger storms implying more latent heat being released (and the converse being true for weaker synoptic activity). This amplification is asymmetrical for the models considered under the simulated $4 \times CO_2$ conditions, due to a greater amount of water vapor contained in warmer air and hence the potential for more condensation for a given synoptic activity. The magnitude of the reduced latent heating is attenuated, whereas increased latent heating is strengthened. Ageostrophic geopotential fluxes are also important in relocating eddy kinetic energy, especially in the vertical.

Corresponding author address: Alexandre Laîné, LSCE/IPSL, UMR CEA-CNRS-UVSQ 1572, CE Saclay, L'Orme des Merisiers, Bâtiment 701, 91191 Gif-sur-Yvette CEDEX, France.
E-mail: alexandre.laine@lsce.ipsl.fr

DOI: 10.1175/2008JCLI2217.1

1. Introduction

In the midlatitudes, especially in winter and for regions influenced by the oceans, the main phenomena determining the meteorology and climate are the synoptic-scale perturbations, the so-called midlatitude storms. These storms form in regions of high baroclinicity (Blackmon 1976; Wallace et al. 1988; Hoskins and Valdes 1990), on the western side of the oceanic basins for the Northern Hemisphere, where a strong temperature contrast exists between land and ocean in a southwest–northeast direction, adding strength to the subtropical westerly jet stream [cf. the thermal wind equation, e.g., Peixoto and Oort (1992)]. As a low pressure system deepens and the associated winds strengthen, moving along the jet stream, a relatively warm and moist air mass is usually advected northward and upward ["warm conveyor belt"; Carlson (1980)], with frontal structures developing at the border between the different air masses. The latent heat released in the air due to greater condensation than evaporation fuels the perturbation, whose effects can be locally as important as baroclinic conversion (Black 1998), although Chang et al. (2002) found a minor energetic role played by moist heating. The rain and snow associated with the fronts are responsible for most of the winter precipitation, which is important for continental hydrology. The behavior of storms at the jet exit where they decay is quite complex and still the focus of active research [cf. results from the Fronts and Atlantic Storm Track Experiment, FASTEX; Baehr et al. (1999)]. Nevertheless, dissipation through friction and barotropic effects is at least among the main dynamical factors.

The local effect of perturbation on winds, temperature, and precipitation also reflects on the global and time-mean scales. The transient eddies significantly contribute to the transport of momentum, heat, and moisture from low to high latitudes, and to the properties of the upper-oceanic layer. The mean climate of the midlatitudes is therefore in part influenced and determined by the eddies, whereas they are themselves influenced and determined by the large-scale and time-mean conditions, through the characteristics of the jet stream and zones of high baroclinicity.

When the potential effects of an increase in greenhouse gases (GHG) on climate are considered, one may expect a larger increase in temperature in the high latitudes compared to the lower ones, at least due to snow and sea ice albedo feedbacks (Moritz et al. 2002; Masson-Delmotte et al. 2005). This general consideration suggests that the jet streams of the winter hemisphere should weaken, as would the synoptic activity due to reduced baroclinicity. Nevertheless, this statement might be too simple considering the strong agreement of the models in also suggesting an increase in the meridional temperature gradient in the upper troposphere under increased GHG concentrations associated with a stronger warming in the tropical upper troposphere (Hall et al. 1994; Solomon et al. 2007). Another potentially important effect is associated with water vapor, since the humidity content of air before saturation increases with temperature [cf. Clausius–Clapeyron equation, e.g., Peixoto and Oort (1992)], leading to potentially more latent heat releasing under increased GHG concentration, which would enhance storm development. Therefore, simple considerations are quite limited in the case of storm track behavior under global climatic change scenarios, and compensation between the different factors cited above may take place. Therefore, simulations using general circulation models (GCMs) are needed in order to consider and understand the potential effects of increased GHGs on storm tracks. However, the representation of storm tracks can be very sensitive to how both the dynamical and physical aspects of the atmosphere are represented in the models, in particular via parameterizations such as those for the convection. Therefore, comparisons between the results of different models are also needed. The aim of this paper is to perform a detailed study of the energetics of storm tracks in two differently behaving GCMs in order to better understand storm track differences between models and the influence of increasing atmospheric humidity on climate change integrations.

The state-of-the-art coupled ocean–atmosphere general circulation models (OAGCMs) participating in the Fourth Assessment Report of the Intergovernmental Panel on Climate Change (IPCC-AR4) suggest a consistent poleward and upward shift of the zonally averaged storm tracks (defined using the eddy kinetic energy), associated with a similar shift in baroclinicity (Yin 2005). Nevertheless, using the same runs (20C and A1B; cf. Solomon et al. 2007) and almost the same years (years 2081–2100 of the A1B scenario, years 1981–2000 or 1961–2000 of 20C), Lambert and Fyfe (2006) do not find significant changes in the spatial distribution of the storm tracks, using the model mean maps of the filtered variance of the 500-hPa meridional wind. The difference should come from the different proxies used to characterize the storm tracks or might result from an artifact of the zonal mean changes used in Yin (2005), which can emphasis differences out of the major storm tracks regions. In terms of frequency and strength of the midlatitude storms, the simulated changes under increased GHG concentrations tend to indicate a reduction in the total number of cyclones but an increase in the number of intense events (Lambert

and Fyfe 2006). This has also been observed in the trends of reanalyses for the second half of the twentieth century (McCabe et al. 2001; Fyfe 2003).

These general conclusions concern model mean behaviors; nevertheless, major differences between models may still exist, especially on a more local scale, which is determinant in terms of local climatic impacts [see, e.g., the results of individual models; Bengtsson et al. (2006); Geng and Sugi (2003)]. In this paper, we focus on two of the IPCC-AR4 models, namely the Institut Pierre Simon Laplace's global coupled model (IPSL-CM4) and the Centre National de Recherches Meteorologiques's coupled ocean–atmosphere model (CNRM-CM3). Under $4 \times CO_2$ concentrations (four times higher than during the preindustrial era), those models show quite similar changes (compared to preindustrial simulations) in the North Pacific sector, but an opposite pattern of behavior over the North Atlantic region (cf. section 3). It is therefore interesting to analyze these changes in order to better understand the dispersion of the models around the multimodel mean. In addition, the focus of this study on only two models allows for an exhaustive analysis of the processes involved.

Our characterization of the transient eddies is based on a time decomposition of the climatic variables (Eulerian method). This allows for the derivation of equations related to the energetics of eddies, which have been used to study single-storm events (e.g., Orlanski and Katzfey 1991; Rivière and Joly 2006a,b), idealized modeling studies (e.g., Chang and Orlanski 1993; Chang and Zurita-Gotor 2007), or the modern climatology of synoptic activity (e.g., Chang et al. 2002). Nevertheless, it had not been used to study the energetics of the storms in simulations with increased GHG concentrations. This framework is particularly relevant in this context since we can consider the separate effects of the different mechanisms entering the dynamics of the storm tracks and relate them to changes in the time-mean conditions. In the case of warmer climates for example, it is particularly interesting to consider to what extent the latent heating is modified due to a greater availability of water vapor, and how this change compares to changes in other energetics conversion terms.

After a brief description of the characteristics of the models and the simulations used for this study (section 2), we focus on the similarities and differences of these two models in terms of changes to the wintertime Northern Hemisphere storm tracks (section 3). We then introduce the eddy energy equations (section 4a), which are used as a basis for our analysis of the storm tracks in the different simulations. The different conversion terms influencing the evolution of the eddy energetics are considered for reanalyzed data, and for the two control simulations (sections 4b and 4c). This highlights the major role of specific mechanisms in the present-day climate and indicates that the models are able to reproduce the physics of the storm tracks despite the relatively low resolution that can affect the representation of storms in the models (e.g., Jung et al. 2006). Section 5 presents an analysis of the changes of the most fundamental conversion terms for the two models under increased GHG conditions, which helps us answer the question of whether the similar and opposite patterns of behavior observed in the two models are due to the same physical processes, or if they can be explained by different contributions from several effects. The last section summarizes the present paper and presents our conclusions.

2. Model and data description

The coupled models used in this study are the CNRM-CM3 (Salas-Mélia et al. 2005) and IPSL-CM4 (Marti et al. 2006). The coupling involves the atmosphere, the ocean, and the sea ice. Vegetation is fixed and set to the present-day distribution.

CNRM-CM3 has been developed by Météo-France. The atmospheric component consists of the third version of the Action de Recherche pour la Petite Echelle et la Grande Echelle (ARPEGE-Climat) model, used with a horizontal spectral resolution of a linear T63 triangular truncation (128×64 grid points and about 2.8° resolution in latitude and longitude) and using 45 layers in the vertical. The oceanic general circulation model is version 8.1 of the Océan Parallélisé (OPA8.1) model, which has an irregular grid, especially in latitude, consisting of 182×152 points in the horizontal and 31 levels in the vertical. The sea ice is obtained with the Global Experimental Leads and Ice for Atmosphere and Ocean (GELATO 2) model, the land surface scheme is based on the Interactions between Soil, Biosphere, and Atmosphere (ISBA) model, the river routing scheme uses the Total Runoff Integrating Pathways (TRIP) model, and the coupling is performed by the Ocean Atmosphere Sea Ice and Soil (OASIS) coupled model, version 2.2. More information on CNRM-CM3 and its general characteristics can be found in Salas-Mélia et al. (2005).

IPSL-CM4 has been developed at the Institut Pierre et Simon Laplace. The atmospheric model (Laboratoire de Météorologie Dynamique, zoom; LMDZ3.3) is a gridpoint model that has a regular horizontal grid of 96×72 points and 19 levels in the vertical. The oceanic model, ORCA2, is also an OPA system, but the grid

(182 × 149 points horizontally, 31 levels in depth) is different from the grid in CNRM-CM3. The sea ice model is the Louvain-la-Neuve Ice Model (LIM), while the Organizing Carbon and Hydrology In Dynamic Ecosystems (ORCHIDEE) model is used for land surfaces, which also includes the river routing scheme, and the coupling is also performed using OASIS (version 3). More information on IPSL-CM4 and its different components can be found in Marti et al. (2006).

The simulations studied in this paper consist of runs performed within the framework of the third phase of the Coupled Model Intercomparison Project (CMIP3) of the IPCC-AR4. The $4 \times CO_2$ runs are initialized from a preindustrial initial state and evolve under increasing CO_2 concentrations of 1% per year until reaching 4 times the preindustrial value. The simulations are then run under this fixed CO_2 concentration for 150 yr. The analyzed years of this study are the last 20 yr of those stabilized $4 \times CO_2$ runs, hereafter referred to as 4CO2.

The control simulations (CTR) consist of the preindustrial runs of each model. We analyze the 20 yr following the same time of integration as in the 4CO2 runs from the same initial conditions. This minimizes the influence of the trends of each model under stable conditions when considering 4CO2–CTR changes. The reanalysis data used to compare the control simulations to observations are taken from the National Centers for Environmental Prediction–National Center for Atmospheric Research (NCEP–NCAR) reanalysis dataset (information online at http://www.cdc.noaa.gov), for the period 1980–99. It has to be kept in mind that the control simulations are preindustrial runs, whereas the climate of the period 1980–99 has already experienced a significant increase in the GHG concentrations compared to the preindustrial levels. Nevertheless, the purpose of this comparison is not to specifically study the differences between the control simulations and the reanalyses, but rather to simply indicate that the models are able to reproduce the major energetic aspects of the storm tracks.

3. Simulated storm tracks changes (4CO2–CTR)

a. Eddy kinetic energy changes

We define the storm tracks using an Eulerian representation. Climate variables are filtered in time in order to isolate their synoptic variations, which are related to the midlatitude perturbations. The filter used is the simple Lorenz's ''poor man's'' filter (Hoskins et al. 1989) used, for instance, in Kageyama et al. (1999) and also commonly used in storm track studies. The winter season is considered (December–February; hereafter DJF). This characterization of the transient eddies has the advantage of allowing the development of eddy energetic equations and studying the different terms of generation, conversion, and dissipation that appear in them (section 4). The quantity used in this section to define storm tracks is eddy kinetic energy (EKE). Other quantities could be used that would lead to similar conclusions. Figures 1a–c represent the storm track fields, averaged from 925 to 200 hPa, for the reanalyses and for the CTR simulations of each model (IPSL-CM4 and CNRM-CM3, respectively), Figs. 1d and 1e present the 4CO2 runs, and Figs. 2a and 2b represent the differences (4CO2–CTR). Vertical sections of the zonally averaged EKE changes are plotted in Fig. 2 for the two OAGCMs along with the CTR field as contours.

Both models simulate the DJF EKE well in terms of localization but are too weak in amplitude (Figs. 1a–c). In terms of simulated changes between the $4 \times CO_2$ and preindustrial climates in the IPSL model (Figs. 1b, 1d, and 2a), the North Atlantic storm track is largely reduced (up to 50%) over the oceanic basin, especially to the south (between 30° and 45°N), corresponding to a poleward shift and reduction in the storm track. For the European region, the synoptic variability is enhanced by around 20% over northern Europe (followed by positive differences all the way across the Eurasian continent north of 45°N), and decreased over the Mediterranean region (by 30% in its eastern part). Concerning the North Pacific storm track, the main changes are found in the eastern part of the basin (east of the date line), with an eastward displacement of the synoptic activity (negative differences between 25°–30°N and 180°–150°W, and positive differences between 30°–45°N and 140°–120°W). Strong positive differences (corresponding up to a 50% increase) are also found over the North American continent, especially in its central part (over the Rocky Mountains and the Great Plains regions) and offshore of its southeastern coast (east of Florida). Note that the enhanced synoptic activity over North America does not influence the North Atlantic storm track, which decreases in strength. The vertical structure of the zonally averaged EKE changes (Fig. 2c) corresponds to an upward and poleward shift of the CTR field, similar to the one found in Yin (2005) (cf. the introduction).

In the CNRM model (Figs. 1c, 1e, and 2b), the changes are weaker than for the IPSL model (as are the absolute values). Contrary to the IPSL model, the North Atlantic storm track is enhanced (up to 30%), especially in its eastern part (east of 50°W) around 45°N. Positive differences are also found extending across central Europe and all the way across Asia around 45°N. For the North Pacific storm track, west of

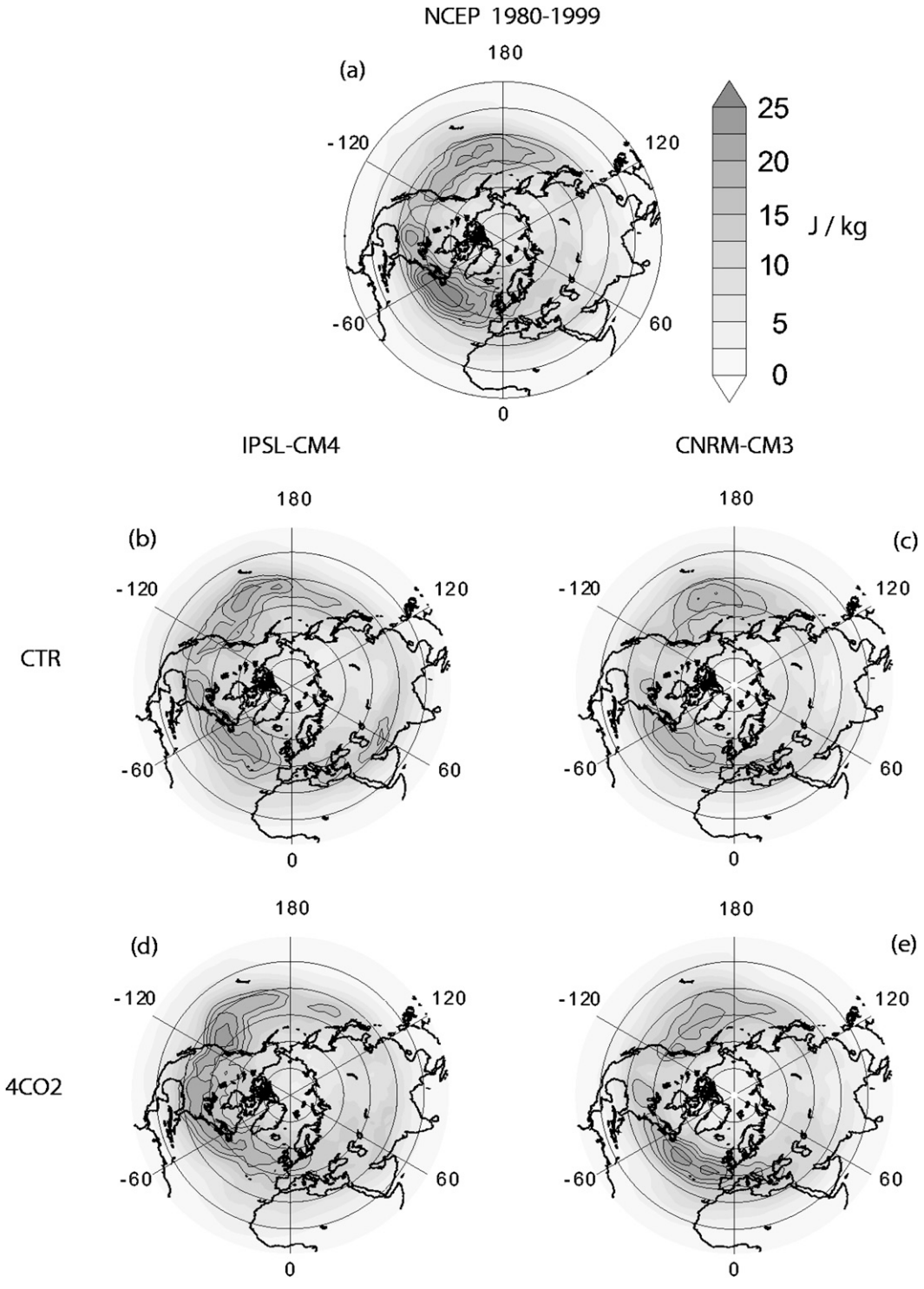

FIG. 1. Eddy (band passed) kinetic energy (J kg^{-1}), averaged from 925 to 200 hPa for DJF means, for (a) NCEP–NCAR reanalyses (1980–99), (b),(d) the IPSL-CM4 model, and (c),(e) the CNRM-CM3 model. (b),(c) CTR simulations, (d),(e) 4CO2 simulations [for EKE greater than 15 J kg^{-1} with contour interval (CI) 2.5 J kg^{-1}].

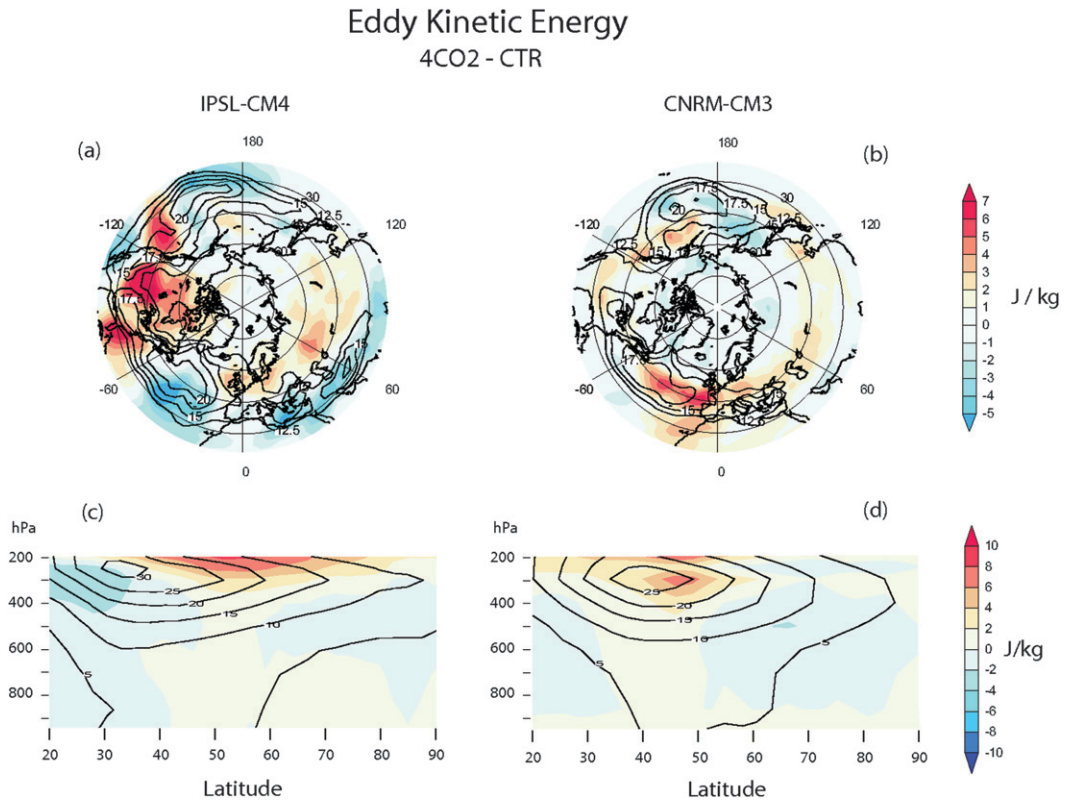

FIG. 2. DJF eddy (band passed) kinetic energy changes (4CO2-CTR), averaged from 925 to 200 hPa, for the (a) IPSL-CM4 model and (b) CNRM-CM3 model. Zonally averaged DJF EKE changes, from 925 to 200 hPa and 20° to 90°N, for the (c) IPSL-CM4 model and (d) CNRM-CM3 model. CTR simulations as isolines, contours every 2.5 J kg^{-1} for EKE greater than 12.5 J kg^{-1} in (a) and (b) and contours every 5 J kg^{-1} in (c) and (d).

the date line, the storm track is slightly enhanced offshore of Japan and reduced to the north (north of 45°N). In its eastern part (east of 180°), there is a northward and eastward displacement of the storm track. Over North America, positive differences are found to the south of the United States (north of 30°N), corresponding roughly to a 20% increase in synoptic activity. The northeastward displacement of the storm track over the eastern Pacific basin and the enhancement over the North American continent are common features of both models, although the details in terms of the amplitude and location of the changes differ. In terms of the vertical structure, Fig. 2d indicates two centers where the differences in EKE are the greatest, one corresponding to a simple poleward displacement and the intensification of the CTR EKE pattern, and the other one corresponding to a poleward and upward shift of the CTR field. Although the pattern is not exactly identical to the one shown in Yin (2005), a poleward and upward shift is also present in this model under increased GHG concentration.

Despite a zonal mean response that is quite consistent in both models, the regions of synoptic activity changes are very different. Therefore, one has to be cautious when interpreting the zonally averaged differences in terms of changes in the main storm tracks of the Northern Hemisphere. Indeed, for both models the storm track changes are not zonally homogeneous, with positive and negative differences compensating at a given latitude, and for the IPSL-CM4 model, the strongest changes are found over the continents and not necessarily over the main storm track regions.

b. *Time-mean baroclinic changes*

To understand the changes between the two climates and the differences between the two models, we first consider time-mean condition changes such as surface temperature 4CO2–CTR differences (Figs. 3a and 3b), which give an indication of the changes in surface baroclinicity when considering the resulting anomalous gradients, and 200-hPa zonal wind changes (Figs. 3c and 3d), which indicates baroclinic changes within the whole troposphere. As expected from general considerations (see the introduction), we notice that the strongest temperature changes are found in the Polar regions (polar amplification) and over the continents (Sutton

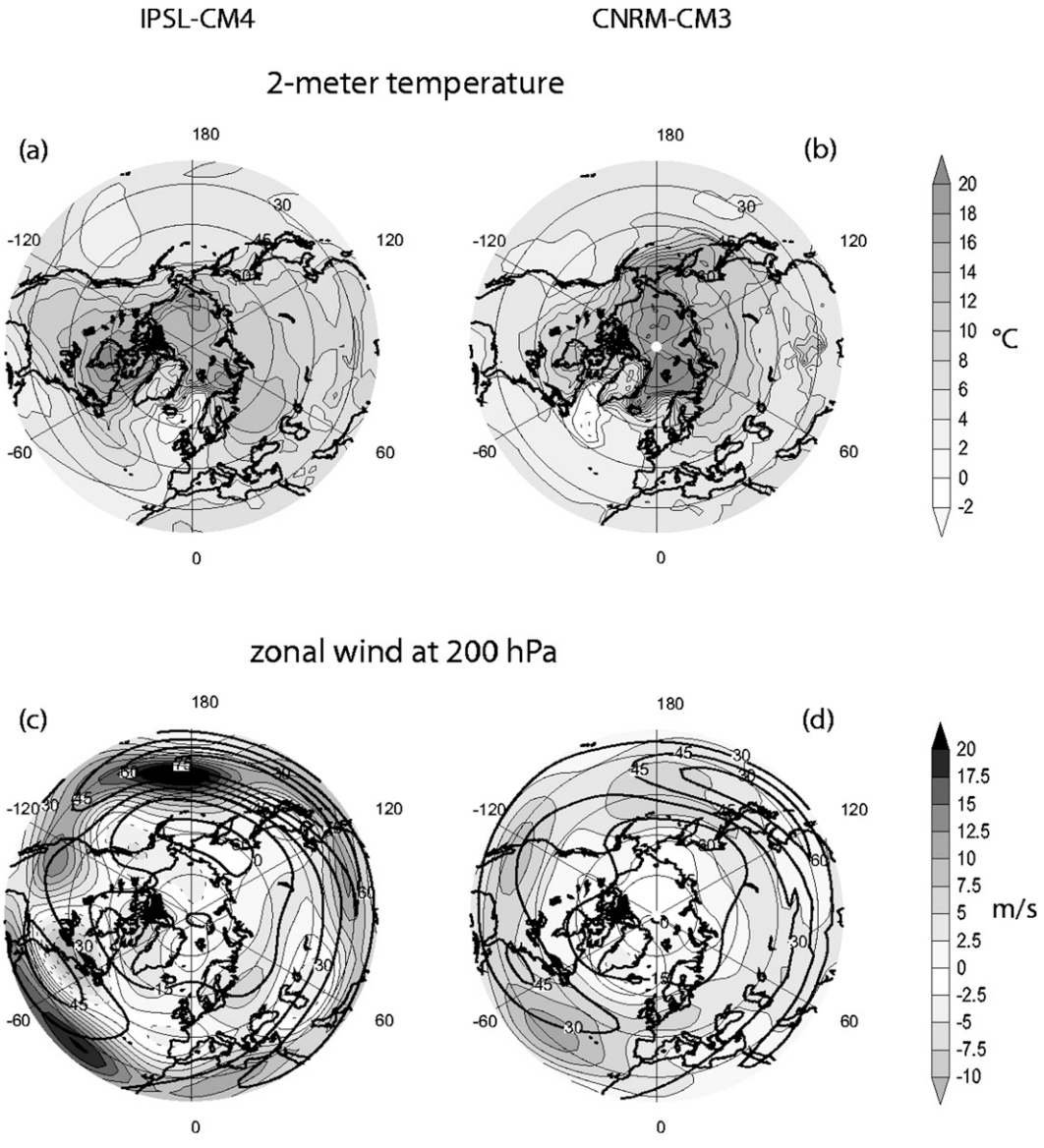

FIG. 3. (a),(b) DJF surface (2 m) temperature changes (4CO2–CTR) (units in °C) and (c),(d) DJF 200-hPa zonal wind differences (units in m s^{-1}) for the (a),(c) IPSL-CM4 model and (b),(d) CNRM-CM3.

et al. 2007). Nevertheless, different structures are found in specific regions that differ from these general north–south, ocean–land warming contrasts. Over the oceans especially, and in specific zones of the North Atlantic subject to sea ice changes, surface temperature differences between the models are large. These zones are particularly important for the storm track behavior and can explain the main differences between the models in terms of synoptic activity changes. For the North Atlantic storm track, the IPSL model simulates a patch of increased surface temperature in the central (in latitude) western basin (around 45°N, west of 30°W), which implies a surface baroclinicity decrease to the south (between 30° and 45°N) and increase to the north (between 45° and 60°N). The synoptic activity itself is indeed reduced to the south and maintained (but not increased) to the north. For the CNRM model, the negative temperature differences found in the Labrador Sea region imply a stronger baroclinicity in the western North Atlantic around 45°N that is consistent with increased synoptic activity. The synoptic activity changes in the North Atlantic are less clearly related to jet stream changes (Figs. 3c and 3d), which therefore suggests that the North Atlantic storm track changes are more closely related to surface baroclinicity changes than to changes occurring higher in the troposphere.

For the western North Pacific region, surface temperature changes seem able to explain part of the observed synoptic activity changes in the CNRM-CM3 model, but not in the IPSL-CM4 model. Over the continents, the surface temperature changes do not explain the synoptic activity changes either, even if jet stream changes there seem spatially correlated with the latter.

Thus, changes in surface baroclinicity and jet stream changes do not explain all the changes in synoptic activity in the 4CO2 simulations compared to CTR. Other factors must therefore play a role. One of the best candidates for further study is latent heat release, which can locally play a role that is as important as baroclinicity in the present-day climate (Black 1998), and which is subject to significant changes in a warmer climate (see the introduction). A more complete picture of the mechanisms involved should help our understanding of the synoptic changes in the different regions of each model and the differences between the two.

4. Eddy energetics: Equations, reanalyses, and CTR simulations

In this section, we present the diagnostics that are used in order to analyze the synoptic activity, and which are based on eddy energy equations. Section 4a presents these equations, whereas sections 4b and 4c consider the terms in the NCEP–NCAR reanalyses and in the CTR simulations, which allows a discussion on the physics involved and the credibility of the models to study storm tracks. Section 5 considers the changes in the major conversion terms influencing the dynamics of the perturbations between the 4CO2 and CTR simulations in each model.

a. Equations

Decomposing the variables into a high-pass part representing transient eddy quantities (denoted by primes) and a low-pass part representing mean-flow conditions (denoted by bars), one can derive the eddy potential (P') and eddy kinetic (K') energy equations in the pressure coordinates [see, e.g., Orlanski and Katzfey (1991) for the eddy kinetic energy equation]:

$$\overline{\frac{\partial}{\partial t}P'} = -\overline{\mathbf{V}}\cdot\nabla_p\overline{P'} - \overline{\mathbf{v}'\cdot\nabla_3 P'} + \overline{\mathbf{F}'}\cdot\overline{\mathbf{T}} + \frac{\mathcal{R}^2}{S_0\Pi(p)}\overline{\theta' Q'} \quad \text{and} \tag{1}$$

$$\overline{\frac{\partial}{\partial t}K'} = -\overline{\mathbf{V}}\cdot\nabla_p\overline{K'} - \overline{\mathbf{v}'\cdot\nabla_3 K'} - \overline{\mathbf{v}'\cdot(\mathbf{v}'\cdot\nabla_3)\overline{\mathbf{V}}} - \overline{F'_{(3)}}\,\overline{T}_{(3)} - \overline{\nabla_3\phi'\mathbf{v}'} + \overline{\mathbf{v}'\cdot\mathcal{F}'}, \tag{2}$$

where $\overline{\mathbf{V}}$ is the mean-flow (two-dimensional, vertical component neglected) and $\mathbf{v}'$ the perturbation wind (three dimensional), and the eddy potential and eddy kinetic energies (noted EPE and EKE, respectively) are

$$P' = \frac{\mathcal{R}^2}{2S_0}\theta'^2; \quad K' = \frac{1}{2}(u'^2 + v'^2),$$

with the reference static stability S_0 depending only on pressure and defined as $S_0 = -\mathcal{R}\partial/\partial p\Theta_0$, with Θ_0 the global mean potential temperature and $\mathcal{R} = R/p_{00}(p_{00}/p)^{c_v/c_p}$ (p_{00} a reference pressure, 1000 hPa in this study), and $\Pi(p) = c_pT/\theta$. Subscripts (3) refer to the third component of the vectors, and $\mathbf{V}_p$ and $\mathbf{V}_3$ to the two- and three-dimensional gradients, respectively.

The first terms on the right-hand side of Eqs. (1) and (2) correspond to the advection of each form of the perturbation energy by the time-mean flow, and the second ones by the eddies themselves. The components of the baroclinic generation term $\mathbf{F}'\cdot\overline{\mathbf{T}}$ are

$$\mathbf{F}' = \mathcal{R}(u'\theta', v'\theta', -\omega'\theta');$$
$$\overline{\mathbf{T}} = \left(\frac{\partial}{\partial p}\Theta_0\right)^{-1}(\partial/\partial x\bar{\theta}, \partial/\partial y\bar{\theta}, -\partial/\partial p\Theta_0),$$

which indicates the role of the eddy heat fluxes in converting energy from time-mean to eddy potential energy through their component parallel to the time-mean temperature gradient. Note that the third component of the vector is also present in the equation of the eddy kinetic energy, but with an opposite sign. This third component is usually negative and in this case represents the conversion of eddy potential to eddy kinetic energy. Note that what is called baroclinic conversion in what follows refers to the scalar product of the first two components of vectors $\mathbf{F}'$ and $\overline{\mathbf{T}}$. The scalar product of the third component is referred to as the conversion term between eddy potential to eddy kinetic energy.

The diabatic heating term, Q, can be decomposed into

$$Q = -\frac{1}{\rho}(\mathrm{div}\mathbf{F}_{\mathrm{rad}} + \mathrm{div}\mathbf{J}^{\mathbf{D}}_{\mathbf{H}}) - L(e-c) + Q_f, \tag{3}$$

with $\mathbf{F}_{\mathrm{rad}}$ the radiative flux, $\mathbf{J}^{\mathbf{D}}_{\mathbf{H}}$ the heat flux due to conduction, L the latent heat of evaporation, e and c the rates of evaporation and condensation, and Q_f the frictional component.

For the eddy kinetic energy equation, the Reynolds stress term $\mathbf{v}'\cdot(\mathbf{v}'\cdot\nabla_3\overline{\mathbf{V}})$ can be decomposed into several parts as in Lackmann et al. (1999):

$$\mathbf{v}'\cdot(\mathbf{v}'\cdot\nabla_3\overline{\mathbf{V}}) = \mathbf{E}'\cdot\overline{\mathbf{D}} - K'\nabla_p\cdot\overline{\mathbf{V}} - \omega'(\mathbf{v}'\cdot\partial/\partial p\overline{\mathbf{V}}),$$

with $\mathbf{E}'\cdot\overline{\mathbf{D}}$ the barotropic generation term, which represents the interaction between the mean-flow barotropy

and the shape of the eddies, and usually dominates the total Reynolds stress term (cf. Lackmann et al. 1999 for term expressions).

The fifth term in Eq. (2) corresponds to the divergence of the ageostrophic geopotential fluxes or the advection by ageostrophic winds of the geopotential synoptic variability. Chang and Orlanski (1993) and Orlanski and Sheldon (1995) show the important role played by this term in the ''downstream baroclinic evolution'' during which an upstream eddy energy center exports energy to a downstream energy center via these geopotential fluxes. The term $\mathbf{v}' \cdot \mathcal{F}$ represents the frictional dissipation.

In our study, we have defined the transient variables denoted by primes in the above equations by filtering daily variables between 2 and 8 days (referred to as bandpass hereafter), whereas the time-mean variables consist of the monthly means. Therefore, a frequency band (hereafter the low-frequency variability) is not considered in this study that should be added to the equations written above, as well as terms representing interactions between the bandpass and the low-frequency parts of the flow. Presenting similar energy budgets for modern storm track energetics, Chang et al. (2002) have decomposed the variables into their monthly mean and the departure from it to be exact with the decomposition considered in the equations. The transient part therefore contains the variability both associated with the activity of the eddies and of the low-frequency variability of the flow. In this study, we have decided to concentrate on the energetics of the eddies (periods between 2 and 8 days) and their changes related to changes in the time-mean conditions (monthly means). The interaction between the eddies and the low-frequency variability is not directly derived but can be partly considered by examining the residue of the potential and kinetic energy budgets. Indeed, for a seasonal-averaged budget as presented hereinafter, the time tendency, and therefore the sum of the generation terms on the right-hand side of the equations, should approximately equal zero. Nevertheless, there are other terms that have not been calculated, which are therefore also present in the residue. This includes the frictional terms, for which we did not have access to the daily output, and the terms of advection by the eddies, which are very noisy.

We did not have direct access to the daily values of latent heating; therefore, we have reconstructed the $(e - c)$ variations from daily means of the specific humidity q and the wind $\mathbf{v}$ on each pressure level following Eq. (12.6) of Peixoto and Oort (1992):

$$\frac{\partial q}{\partial t} + \nabla_3 \cdot \mathbf{v}q = (e - c). \tag{4}$$

This reconstruction of latent heating is subject to errors. In particular, the calculation of the time tendency of the specific humidity is quite sensitive to the time step used. A derivation of the latent heating following this formula has been tested on the NCEP–NCAR reanalyses from daily values of specific humidity (as used in this study) and from 6-h ones, which indicates differences as large as 20%. Despite the uncertainty on the exact figure of the latent heating term, we consider our estimate to give a relevant order of magnitude of the term and that the differences in the diabatic generation term associated with the moist effects simulated by the models between the two climates contain relevant information.

The different conversion terms are presented in the next two subsections, with a computation for the NCEP–NCAR reanalysis variables and the two CTR simulations. We consider the DJF averages of the different conversion terms governing the energetics of the perturbations at each grid cell of the models.

b. Eddy potential energy conversion terms

Figure 4 shows the different conversion terms contributing to the increase or decrease of EPE, integrated from 925 to 200 hPa for nonsurface processes, averaged between 25° and 60°N, and shown as a function of longitude. The values for each process then represent the mean energy transferred in 1 s to a 1-m^2 column of air in the troposphere at the given longitude. Note that for the sensible fluxes, the factor $\mathcal{R}^2/S_0\Pi(p)$ has not been strictly calculated at the surface since it necessitates the calculation of a derivative in pressure in S_0 and since the variables are only available on given pressure levels. Instead, its mean value is calculated between 1000 and 850 hPa. For the radiative heating term, only the vertical derivative of the radiation flux has been considered, and div ($\mathbf{F}_{\text{rad}}$) has been derived from the daily difference between the net radiation emitted at the surface and the one emitted at the top of the atmosphere and θ consists of the daily mean potential temperature in the troposphere (1000–200 hPa). For the rest of the terms, the different components are calculated at each pressure level.

1) REANALYSES

The two main storm tracks clearly appear in the reanalyses data (Fig. 4a) as maxima of the baroclinic (red curve), latent heating by excess of condensation versus evaporation (dark blue curve), and EPE to EKE conversions (green curve) in the regions around 60°W and 160°E. Among the different mechanisms considered,

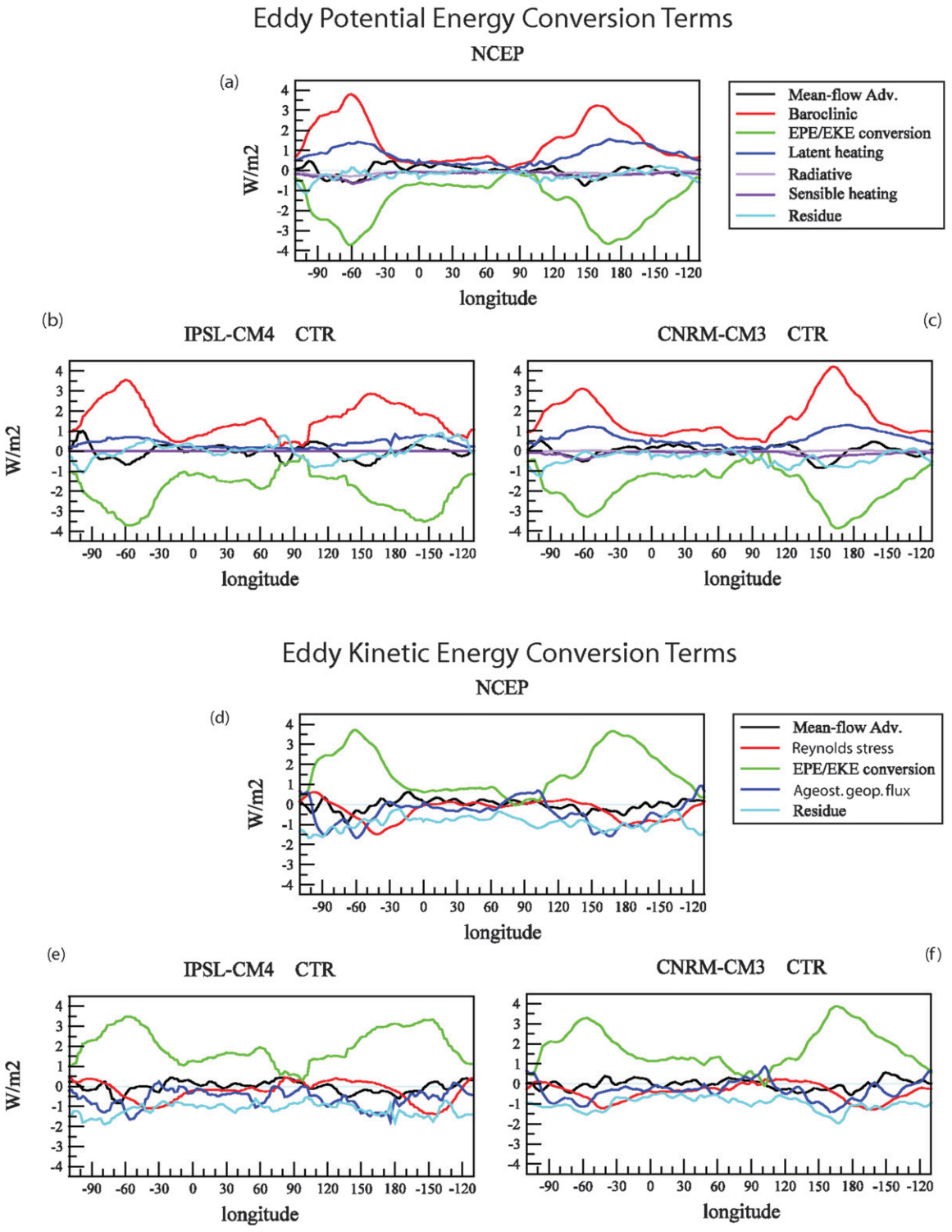

FIG. 4. DJF eddy (band passed) potential energy conversion terms [cf. Eqs. (1) and (3)] and DJF eddy kinetic energy conversion terms [cf. Eq. (2)] integrated from 925 to 200 hPa (except for terms related to surface fluxes), averaged from 25° to 60°N for (a),(d) NCEP reanalyses, (b),(e) the IPSL-CM4 CTR run, and (c),(f) the CNRM-CM3 CTR run. Units in W m^{-2}.

these three are found to be dominant for the EPE budget. The orders of magnitude of the mean-flow advection (black curve in Fig. 4a) and the radiative (brown curve) and the sensible heating (purple curve) are smaller. The residue of the budget (light blue curve in Fig. 4a) is very close although not strictly equal to zero. This can be due to advection by the eddies that is not included in the budget; to interaction with the energetics of the low-frequency part of the flow, which is also not considered; and/or to discrepancies in our estimates of the different terms, especially the latent heating term through our reconstruction of the daily variations of $(c - e)$, or the sensible heat flux through our estimate of S_0 at the surface (cf. previous sections). Considering the fact that the mean circulation flows eastward for this band of latitude, we also get an idea of the chronology of the different mechanisms taking place in the cyclogenesis and cyclolysis.

For the North Atlantic storm track, the conversion from mean-flow to eddy potential energy through baroclinic effects (red curve in Fig. 4a) starts to take place around 110°W, before peaking at about 3.75 W m^{-2} around 60°W, which corresponds to the longitude of the eastern coast of the North America, where cyclogenesis is known to be very intense (Hoskins and Hodges 2002). East of 60°W, baroclinic conversion strongly diminishes. The energy received from condensation (dark blue curve in Fig. 4a) reaches its maximum values of about 1.5 W m^{-2} around 50°W, but stays at similar levels east of it. This suggests that latent heating is still active during the mature phase of storms, after the baroclinic conversion has ceased. The baroclinic conversion is always predominant in the creation of eddy potential energy, except at the storm track's end where it is equivalent to the synoptic latent heating.

For the North Pacific storm track, the same general conclusions are found. Baroclinic conversion dominates the creation of eddy potential energy, and increases from 80°E eastward, with a local maximum around 120°E and the primary peak of about 3.25 W m^{-2} found at around 160°E. East of it, baroclinic conversion decreases regularly, although less quickly than in the North Atlantic, at a rate of about 0.04 W m^{-2} (° longitude)$^{-1}$. Latent heating starts increasing at about 120°E, the western longitude of the Japan Sea. It reaches a peak in creating eddy potential energy of about 1.5 W m^{-2} at 170°E, east of which moist heating stays at a level of about 1 W m^{-2} over the eastern North Pacific and equals the creation of eddy energy through baroclinic conversion east of 160°W. Therefore, for each storm track, the dominant mechanism that creates eddy potential energy is baroclinic conversion, with latent heating contributing less to the energetics budget and slightly later in the eddy life cycle, during the mature phase of the perturbations.

Compared to the results of Chang et al. (2002), who performed a similar quantification of the eddy energy conversion terms from NCEP–NCAR reanalyses for the period 1980–93, we find a greater role for the latent heating with respect to baroclinic conversion. The ratio of the former to the latter is of the order of one-half to one-third in our case compared to about one-fifth in Chang et al. (2002). Several differences nonetheless exist between our two analyses. They consider January months compared to DJF in our case, and their definition of the static stability seems local [cf. their Eq. (5)] rather than global, as in ours. Also, transient quantities consist of deviations from the monthly means in their case compared to 2–8-day variability in our analysis. Finally, their computation of the latent heating rate and ours differ, and may in both cases lead to discrepancies.

Simultaneously to these two major EPE generation effects, removal of this energy occurs through conversion into EKE, at a rate almost equal to the sum of the two main EPE creation terms. In fact, the conversion term from eddy potential to eddy kinetic energy is associated with a vertical movement correlated (at synoptic scale) to temperature changes. The conversion is from eddy potential to eddy kinetic energy when $-\omega'\theta'$ is positive, that is, when the ascent of air is synoptically associated with a warming, for example, either (a) when the ascent of air transports warm air or (b) when warming air implies an ascent (and the contrary for sinking air masses). Frontogenesis usually starts with a cross-frontal circulation at the early stage of cyclogenesis, with air rising on the warm side of the front and air sinking on the cold side of the front (e.g., Hoskins and Bretherton 1972). The situation corresponds to the first case described above. For latent heating, the mechanism involved is condensation along the fronts during the developing and mature stages of the storms, when ascending motion of moist air gives rise to condensation and, therefore, to a heat release that further contributes to the vertical movement of air.

2) MODEL EVALUATION

Figures 4b and 4c indicate that the energetics of the storm tracks are well reproduced in the CTR simulations, when compared to the reanalyses, at least in terms of the localization of the physical processes involved and their relative contributions. Compared to the reanalyses, the IPSL CTR simulation (Fig. 4b) simulates a realistic baroclinic conversion term for the North Atlantic storm track and the western North Pacific (slightly weaker by a few percent), whereas it is too

strong in the eastern North Pacific, east of the date line. The latent heat released into the air is about 50%–60% too weak in the model and the peak found in the North Pacific is simulated too far eastward. The conversion from eddy potential to kinetic energy is similar to reanalyses in the North Atlantic, whereas it peaks too much to the east, around 150°W instead of 170°E in the North Pacific.

The CNRM CTR model simulates realistic patterns of generation terms. The latent heating term is very similar in shape and magnitude to the one found from reanalyses, whereas the baroclinic conversion peak is too weak in the North Atlantic (by about 20%) and too strong in the North Pacific (by about 25%).

This broad consistency of the models with respect to the reanalyses gives us confidence in their ability to simulate the dynamics of storm tracks. In a $4 \times CO_2$ context, in which we can expect latent effects to be significantly modified, we should pay attention to the biases related to this factor, which are particularly large in the IPSL model compared to the CNRM model. Nevertheless, the primary factor of eddy energy generation is baroclinic conversion, which the models simulate relatively well.

c. Eddy kinetic energy conversion terms

Figure 4d shows the different eddy kinetic advective and conversion terms, also integrated from 925 to 200 hPa and averaged between 25° to 60°N, for the NCEP–NCAR reanalyses. The generation of EKE is almost entirely due to the conversion from eddy potential to eddy kinetic energy (green curve). Concerning the mechanisms removing or destroying EKE locally, the ageostrophic geopotential flux term (dark blue curve in Fig. 4d) and the Reynolds stress term (red curve) are both important. The dissipation of eddy kinetic energy through friction is not considered but could be of a magnitude similar to the two latter terms, if we consider that the major part of the residue term (light blue curve in Fig. 4d) is due to this mechanism. The advection term (black curve in Fig. 4d) is comparatively less important.

During a first phase (100°–60°W for the North Atlantic storm track, 100°–170°E for the North Pacific storm track), EKE is mostly removed through the divergence of ageostrophic geopotential flux (1–1.5 W m^{-2} removal). Eddy energy is redistributed from the entrance region of the storm tracks, where baroclinicity is strong, toward the exit region of the storm tracks, where it helps maintain eddy activity [''downstream development''; Chang and Orlanski (1993); Orlanski and Sheldon (1995)]. It may come as a surprise that only slightly positive or null values are found in the exit region of the storm tracks (eastward of 30°W in the North Atlantic and eastward of 150°W in the North Pacific), where the geopotential flux is supposed to be converging. This is due to the fact that regions of flux convergence are compensated by regions of flux divergence for the same longitude in most part of the 25°–60°N band in the exit regions of the storm tracks (not shown). It is also consistent with Fig. 10b in Chang and Orlanski (1993) and its interpretation by the authors: eddies that grow from flux convergence also partly decay through divergence of geopotential fluxes, therefore explaining the small net amplitude and the large spread of regions of flux convergence when averaged in time. During a second phase (peaking at 40°W in the North Atlantic and east of 180° for the Pacific), the predominant net destructive effect occurs through barotropic conversion (which dominates the Reynolds stress term; not shown), reaching values higher than 1 W m^{-2}. Black and Dole (2000) showed that at the entrance of the storm tracks, the typical north–south extension of the perturbations interacts constructively with the stretching of the mean flow. This corresponds to the slightly positive values observed at the very beginning of the storm tracks in Fig. 5. Farther downstream, the interaction between the eddies and the shear of the mean flow (on lateral sides of the core of the jet), or the mean-flow stretching at the jet's end, tend to destroy the eddies. This is what is observed in the plots with the negative values of the Reynolds stress term.

As for the EPE conversion terms, the ones for the eddy kinetic energy simulated by the IPSL and CNRM models (Figs. 4e and 4f, respectively) are at first order very similar to the reanalyses. The patterns of EKE removal through ageostrophic geopotential flux divergence are well simulated, although the absolute values are in general slightly weaker in the models, especially in CNRM-CM3. As for the eddy potential energetics, the eastern Pacific is the region of higher bias in terms of eddy kinetic removal, with a peak in barotropic EKE destruction that is slightly stronger than in the reanalyses and shifted eastward in both models, especially in IPSL-CM4.

5. Changes in eddy energetics (4CO2–CTR)

In this section, we analyze and discuss the changes simulated by each model separately in terms of the EPE and EKE conversion terms. Longitudinal plots are used to compare the relative changes of all factors. Maps of the differences for the main factors are used in order to consider the spatial structures of the changes. Vertical sections of zonally averaged differences are also plotted to complete the picture.

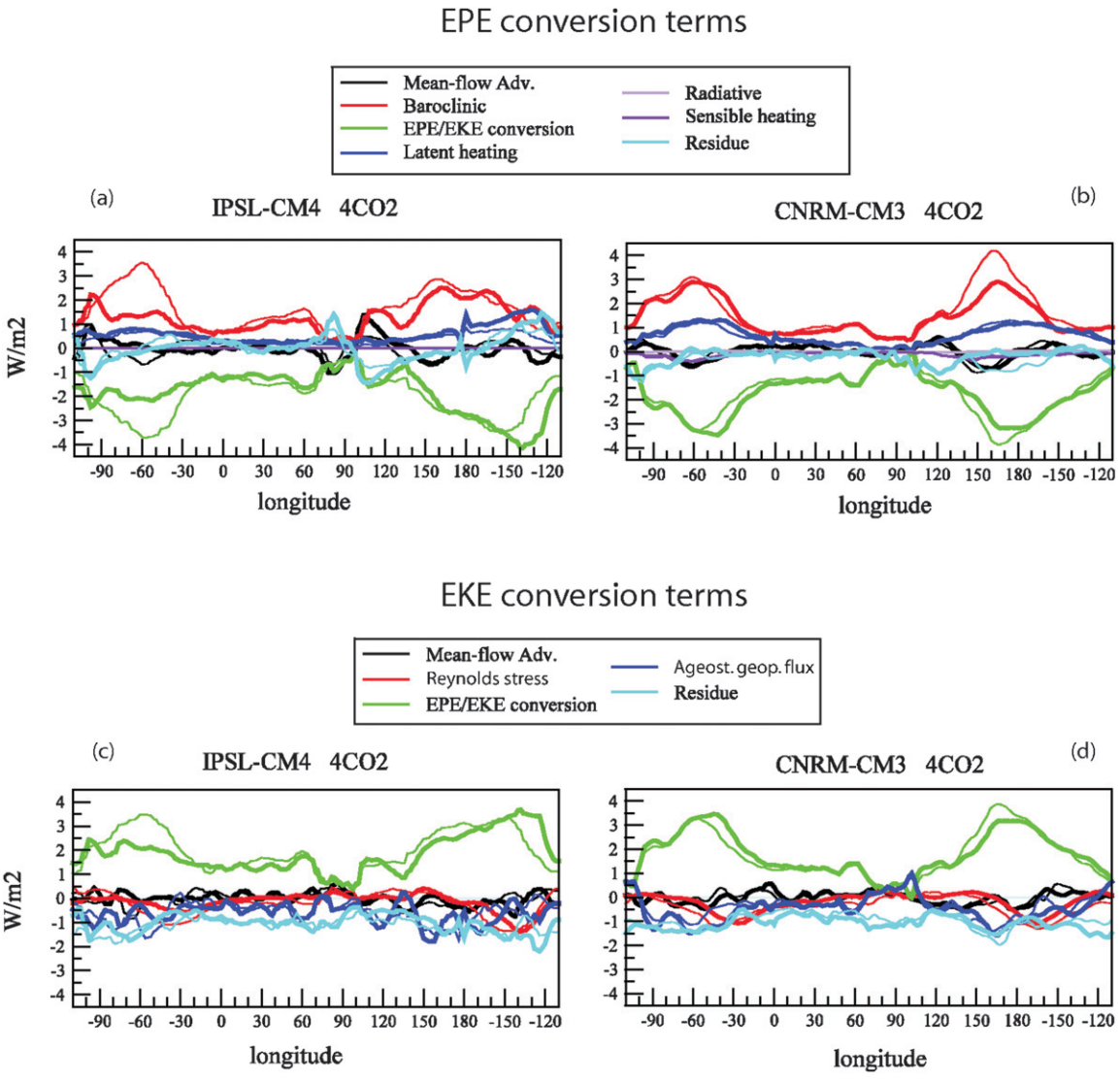

FIG. 5. (a),(b) DJF eddy potential energy conversion terms and (c),(d) eddy kinetic conversion terms integrated from 925 to 200 hPa (except for surface fluxes related terms), averaged from 25° to 60°N for (a),(c) IPSL-CM4 and (b),(d) CNRM-CM3. Thick lines for the 4CO2 runs, thin lines for the CTR runs. Units in W m^{-2}.

a. IPSL-CM4 model

1) NORTH ATLANTIC STORM TRACK

Figure 5a shows the EPE conversion terms, plotted longitudinally as in Fig. 4, for the 4CO2 runs of the IPSL model. Thin lines represent the CTR values of the different terms. The baroclinic generation term of the North Atlantic storm track has been strongly reduced (about 60%) in the 4CO2 run of the IPSL model. It is consistent with the simulated temperature changes plotted in Fig. 3a. A slight peak in baroclinic generation still exists over central North America around 100°W but is not maintained and enhanced in the main baroclinic region of the CTR run along the eastern coast of the continent.

To precisely quantify what is responsible for the simulated changes in baroclinic generation, we have plotted the relative contribution of the changes in the mean vertical stratification, eddy heat flux magnitude, mean horizontal gradient, and the angle between the eddy heat flux and the mean temperature gradient. Indeed, $\mathbf{F}'_\mathbf{H} \cdot \overline{\mathbf{T}}_\mathbf{H} = \mathcal{R}^2 \times (1/S_0) \times |\theta'\mathbf{v}'| \times |\nabla\overline{\theta}| \times \cos(\theta'\mathbf{v}', \nabla\overline{\theta})$ (the subscript H corresponds to the horizontal component of a vector), from which we define $\alpha_{tot} = \alpha_1 \times \alpha_2 \times \alpha_3 \times \alpha_4$, with α_{tot} referring to the ratio between the 4CO2 and the CTR values of $\mathbf{F}'_\mathbf{H} \cdot \overline{\mathbf{T}}_\mathbf{H}$ and α_i referring to the ratios of $1/S_0$, $|\theta'\mathbf{v}'|$, $|\nabla\overline{\theta}|$, and $\cos(\theta'\mathbf{v}', \nabla\overline{\theta})$. Figure 6 shows the longitudinal relative contributions to the changes in baroclinic

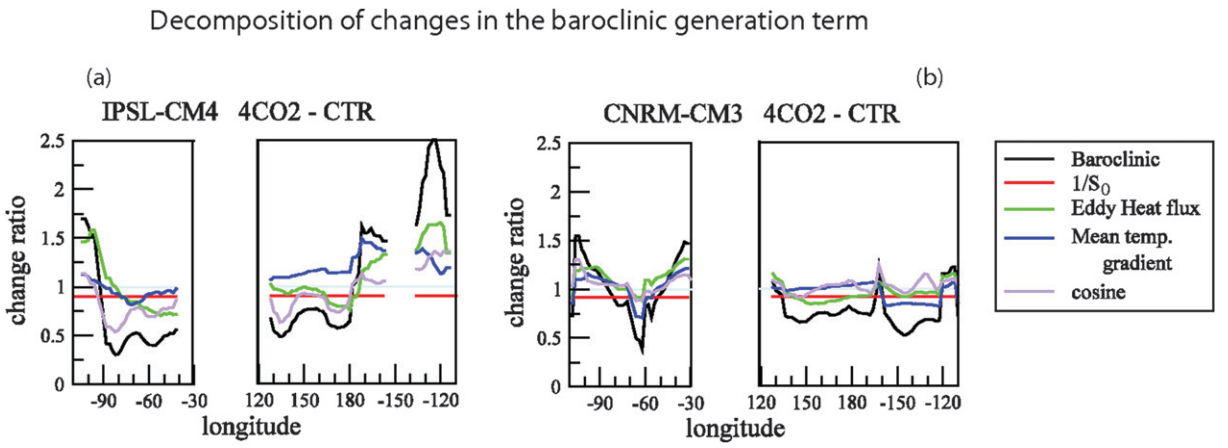

FIG. 6. DJF change ratio (4CO2/CTR), integrated from 925 to 200 hPa, averaged from 25° to 60°N, for $\mathbf{F}_H \cdot \overline{\mathbf{T}}_H$ (α_{tot} in text, black line), $1/S_0$ (α_1, red line), $|\theta'\mathbf{v}'|$ (α_2, green line), $|\nabla\overline{\theta}|$ (α_3, blue line), and $\cos(\theta'\mathbf{v}', \nabla\overline{\theta})$ (α_4, brown line). Note that vertical integration was performed prior to the derivation of the ratio for clarity. Also, the values have been considered only in regions where baroclinic conversion term differences (4CO2–CTR) were superior to 1 for the IPSL model and 0.5 for the CNRM model in order to isolate the regions of interest and remove the noise induced by the cosine change ratio outside of these zones.

generation, that is, the DJF means of α_i, integrated from 925 to 200 hPa, averaged from 25° to 60°N. Note that the product of the different α_i in Fig. 6 (not shown) is close to α_{tot} despite the averages and the vertical integration performed, allowing for an interpretation of α_{tot} in terms of the different α_i plotted. Also note that in these plots, the values have only been considered in the areas where the absolute value of (4CO2–CTR) the baroclinic differences is superior to 1 W m^{-2} for the IPSL model, and 0.5 W m^{-2} for the CNRM model. This corresponds to the regions of the main storm tracks (Figs. 7a and 7b) and was performed because the ratio of $\cos(\theta'\mathbf{v}', \nabla\overline{\theta})$ outside the zones of interest can take large values and completely mask the relevant information in the meridional averages.

For the North Atlantic storm track in the IPSL model, the change in baroclinic generation between 90° and 60°W (Fig. 6a, left panel) can be mostly attributed to a change in the angle of the eddy heat flux with the mean temperature gradient (α_4; brown line in Fig. 6a). The efficiency of the eddies to take energy from the mean flow may be reduced due to changes in the shape and orientation of the eddies. The changes in the eddy heat flux (α_2; green line in Fig. 6a) are also an important parameter influencing the changes in baroclinic development and can be interpreted as a nonlinear effect or positive feedback, since more synoptic activity implies more eddy heat flux, which itself implies more baroclinic conversion and hence more synoptic activity. A global increase in static stability tends to reduce the baroclinic conversion everywhere (α_1; red line in Fig. 6a). The mean temperature gradient changes (α_3; blue line in Fig. 6a) also have an effect on α_{tot} (black line), although it is not the main direct factor. Nevertheless, it can be indirectly responsible for eddy shape changes, especially through the role played by the jet intensity on the eddies, in particular through the kind of elongation and wave breaking that it can induce (Orlanski 2003; Rivière and Orlanski 2007).

The EPE generation through latent heating still peaks in the North Atlantic storm track, contrary to the baroclinic generation term, and is almost unchanged compared to the CTR simulation when meridionally averaged (Figs. 5a). Looking at maps of latent heating changes (Fig. 7c), we notice that there is a slight reduction in moisture generation south of 45°N and a slight increase north of it, consistent with a northward shift of the North Atlantic storm track in the IPSL model (Figs. 1b, 1d, and 2a).

As already discussed for the CTR runs and reanalyses (section 4b), depending on the stage of development of the eddies, the EPE generation processes through baroclinic (early stage) or the latent heating (mature stage) involve vertical movements related to eddies, and help generate EKE. The conversion from EPE to EKE therefore counterbalances the EPE generation through baroclinic or latent heating depending on the region considered, as for the CTR simulations (Fig. 5a).

The EKE conversion terms are plotted in Figs. 5c and 5d in the same way as in Figs. 5a and 5b but for EPE. Concerning the North Atlantic for IPSL-CM4, Fig. 5c shows that the 4CO2 EKE removal through ageostrophic advection of geopotential eddy centers or destruction through barotropic effects (Reynolds stress term) is reduced compared to the CTR run, which

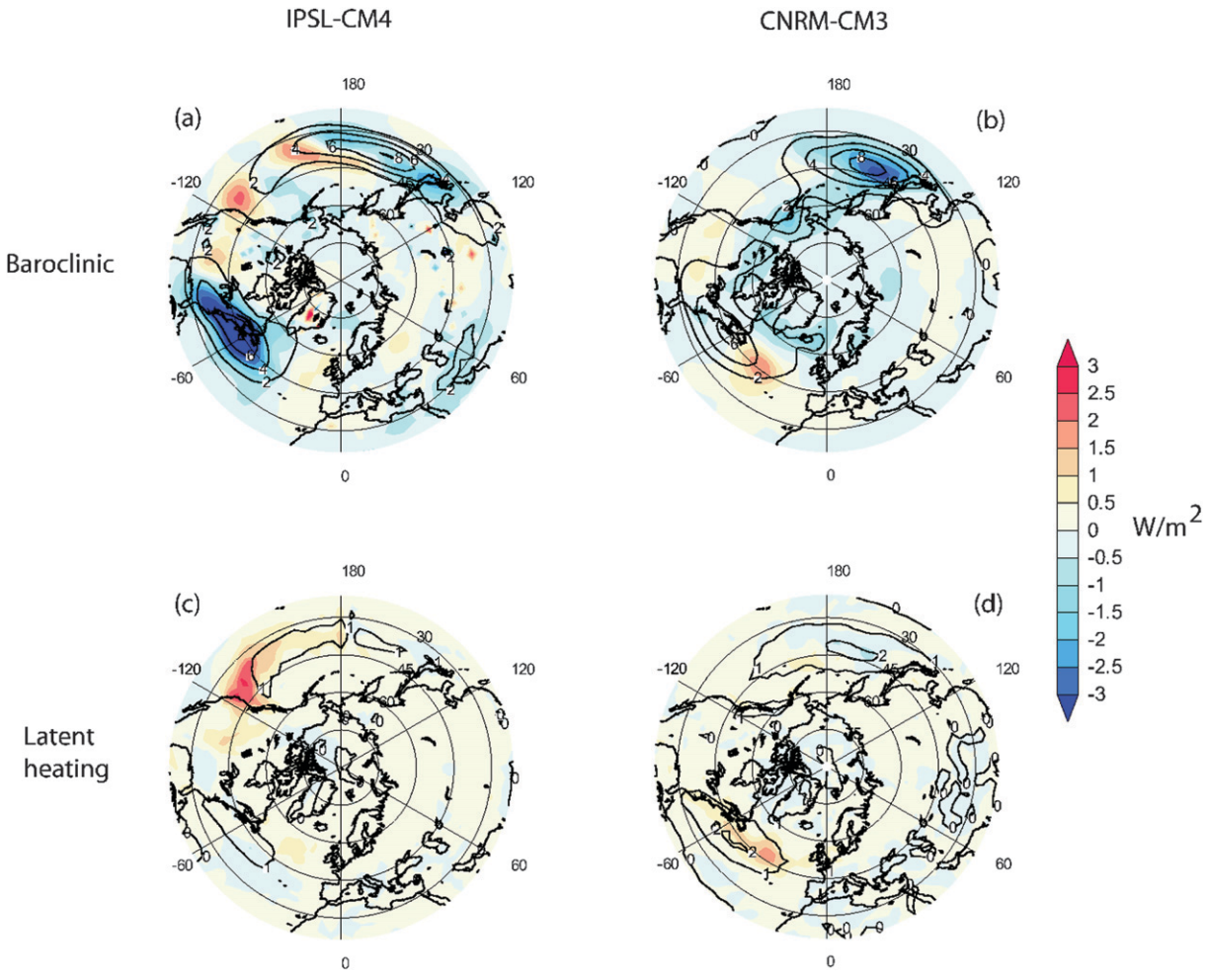

FIG. 7. Main DJF EPE generation term, integrated from 925 to 200 hPa, for the (left) IPSL-CM4 model and (right) CNRM-CM3 models. (a),(b) The baroclinic generation term; (c),(d) the eddy latent heating term (not including the surface latent flux). CTR simulations as isolines, CI 2 W m^{-2} in (a),(b) and CI 1 W m^{-2} in (c),(d). The 4CO2 − CTR differences are shown in color.

corresponds to positive differences on the maps in Figs. 8c and 8e. Synoptic activity is reduced; therefore, the absolute value of the energy loss is also reduced.

2) NORTH PACIFIC STORM TRACK

The North Pacific storm track changes mostly in its eastern part, with an eastward displacement of the EKE (Fig. 1). In fact, Fig. 7a shows that there is a constant reduction by 1–2 W m^{-2} of baroclinic generation over the whole western North Pacific (west of 180°). This generation loss can explain the reduced synoptic activity in the first part of the eastern Pacific, between 170°E and 150°W (Fig. 2a). This reduced baroclinic transfer is not due to a reduced mean temperature gradient but rather to a reduced efficiency of eddies to convert energy from the mean flow due to changes in the angles between the eddy heat fluxes and the mean temperature gradient (Fig. 6a). Downstream, the eastward enhancement of the storm track is associated with latent heating processes, with eddy energy generation differences that are greater than 1 W m^{-2} when meridionally averaged (Fig. 5a) and up to 2.5 W m^{-2} locally (Fig. 7c). Baroclinic conversion changes contribute equally to the eastward enhancement of the energy generation around 130°W (Figs. 5a and 7a).

The EPE transferred to EKE is then still removed first, predominantly through ageostrophic geopotential flux and then through barotropic effects (Fig. 5c). In terms of changes (Figs. 8c and 8e), in the far eastern North Pacific, the differences in EKE removal (related to the fact that synoptic activity is enhanced) are mostly associated with the enhanced divergence of geopotential fluxes rather than with barotropic processes changes.

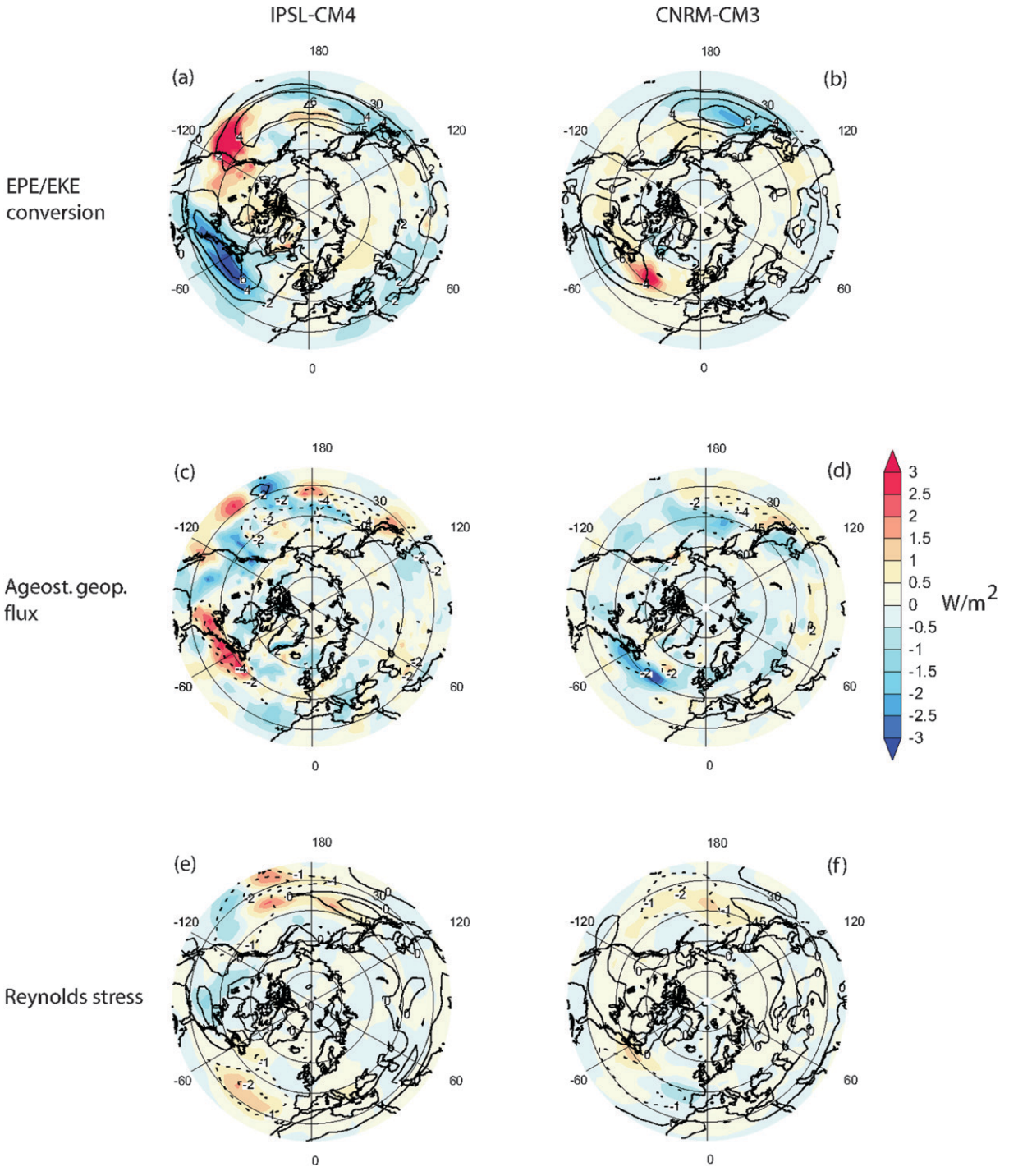

FIG. 8. Main DJF EKE conversion term, integrated from 925 to 200 hPa, for the (left) IPSL-CM4 and (right) CNRM-CM3 models. (a),(b) The EPE to EKE conversion term; (c),(d) EKE removal through ageostrophic geopotential flux; and (e),(f) the Reynolds stress. Shown are CTR simulations as isolines, CI 2 W m^{-2}, except for the Reynolds stress(CI 1 W m^{-2}). [Note that the 0 isoline is removed in (c) and (d) for clarity.] The 4CO2 − CTR differences are shown in color.

3) VERTICAL STRUCTURE

We have considered the horizontal changes of the conversion terms. We now consider the vertical structure of the changes in order to understand the poleward and upward shift of the zonally averaged EKE shown in Fig. 2c and also noticed in Yin (2005). Figure 9 shows the zonally averaged changes in the EPE and EKE generation terms along with the CTR values as contours. Although the changes are not zonally uniform, rendering the interpretation of zonally averaged fields difficult, the specificity of the changes makes it possible. Indeed, in the IPSL model, the negative differences in the baroclinic generation that dominate the vertical means in Fig. 7a are found in the lower part of the troposphere and extend deep into it, whereas the positive differences are mostly restricted to the uppermost part of the troposphere (above 300 hPa; not shown). We therefore have an idea of where the changes observed on the vertical section belong on the horizontal section.

For the CTR run (contours), we find two maxima centers in the vertical in the baroclinic generation term (Fig. 9a), peaking at about 5×10^4 W kg^{-1}. These two centers in the vertical are not separated geographically and are found in the regions of storm formations on the western sides of the oceanic basins. There is only one center of maximum baroclinic generation in the NCEP–NCAR reanalyses (peaking at about 4.5×10^4 W kg^{-1}), which extends from the surface deep into the troposphere, at roughly the same location as in the models (not shown). The negative differences in the IPSL model for this baroclinic term are found in the lower troposphere (below 350 hPa), with a peak at -1.25×10^4 W kg^{-1}, whereas positive differences are located in the uppermost part of the troposphere, peaking at 2×10^4 W kg^{-1} at 200 hPa. Note that positive differences are also found in the upper troposphere for regions where the vertical-mean baroclinic conversion is dominated by negative differences in the lower troposphere (western sides of the oceanic basins in the IPSL model; cf. Fig. 7a), therefore representing an upward shift of the baroclinic conversion. Latent heating, which mainly peaks in the central part of the troposphere at about 1.5×10^4 W kg^{-1} for the CTR run, is enhanced in the 4CO2 runs (Fig. 9c) and is shifted poleward and upward. The pattern of conversion from EPE to EKE (Fig. 9e) is broadly consistent with the two main generation terms discussed above, with the CTR values peaking in central part of the troposphere (around 500 hPa) with values around 6×10^4 W kg^{-1}. Note that sensible heat fluxes, whose values are weak in terms of the energy budget for the whole tropospheric air column, are important for the surface EPE budget where it should remove potential energy from the eddies. In the 4CO2 case, the EPE to EKE conversion is decreased equatorward and downward by up to -1.2×10^4 W kg^{-1}, associated with the baroclinic conversion term, and enhanced poleward and upward by up to 2×10^4 W kg^{-1}, which is mostly associated with the changes in the baroclinic and latent heating generation of EPE. The input of energy from EPE to EKE is displaced by the ageostrophic geopotential fluxes from the central part of the troposphere to the upper part (above 300 hPa) and at the surface (below 900 hPa; cf. contours in Fig. 9g). The EKE at the surface must be removed by surface friction that had not been calculated explicitly. In the upper part of the troposphere, the poleward and upward enhancement of energy input is displaced even farther poleward and upward by the ageostrophic geopotential fluxes (Fig. 9g). Barotropic conversion has a diminished impact on the EKE budget (Fig. 9i). Therefore, the main processes involved in the poleward and upward shift of zonally averaged EKE are baroclinic conversion (concerning mainly an upward enhancement), latent heating, and relocation by geopotential fluxes.

b. CNRM-CM3 model

1) NORTH ATLANTIC STORM TRACK

Figure 5b shows that the EPE generation in the eastern part of the North Atlantic storm track (east of 50°W) is slightly increased in the 4CO2 simulation of the CNRM model compared to the CTR run. The changes in the baroclinic conversion results from equivalent changes in all of the components of the baroclinic generation rate term (Fig. 6b). Compared to the IPSL model, the direct effect of the mean temperature gradient intensity is more pronounced, whereas the effect of the change in the cosine term is less important (Figs. 6a and 6b). The generation of EPE through moist effects also increases in the eastern part of the storm track by about the same order of magnitude as the baroclinic conversion (Figs. 5b, 7b and 7d).

In terms of the EKE budget, the enhanced synoptic activity in the 4CO2 run (Fig. 2b) is due to an increase in EPE to EKE energy conversion (Fig. 5d). This increase in synoptic activity is associated with an enhanced local removal, which occurs through ageostrophic geopotential advection processes (Figs. 8d and 8f).

2) NORTH PACIFIC STORM TRACK

The EKE changes in the North Pacific consist of a slight increase in the western Pacific on the southern edge of the storm track and a significant reduction on the northern edge (Fig. 1c). In the eastern Pacific, the

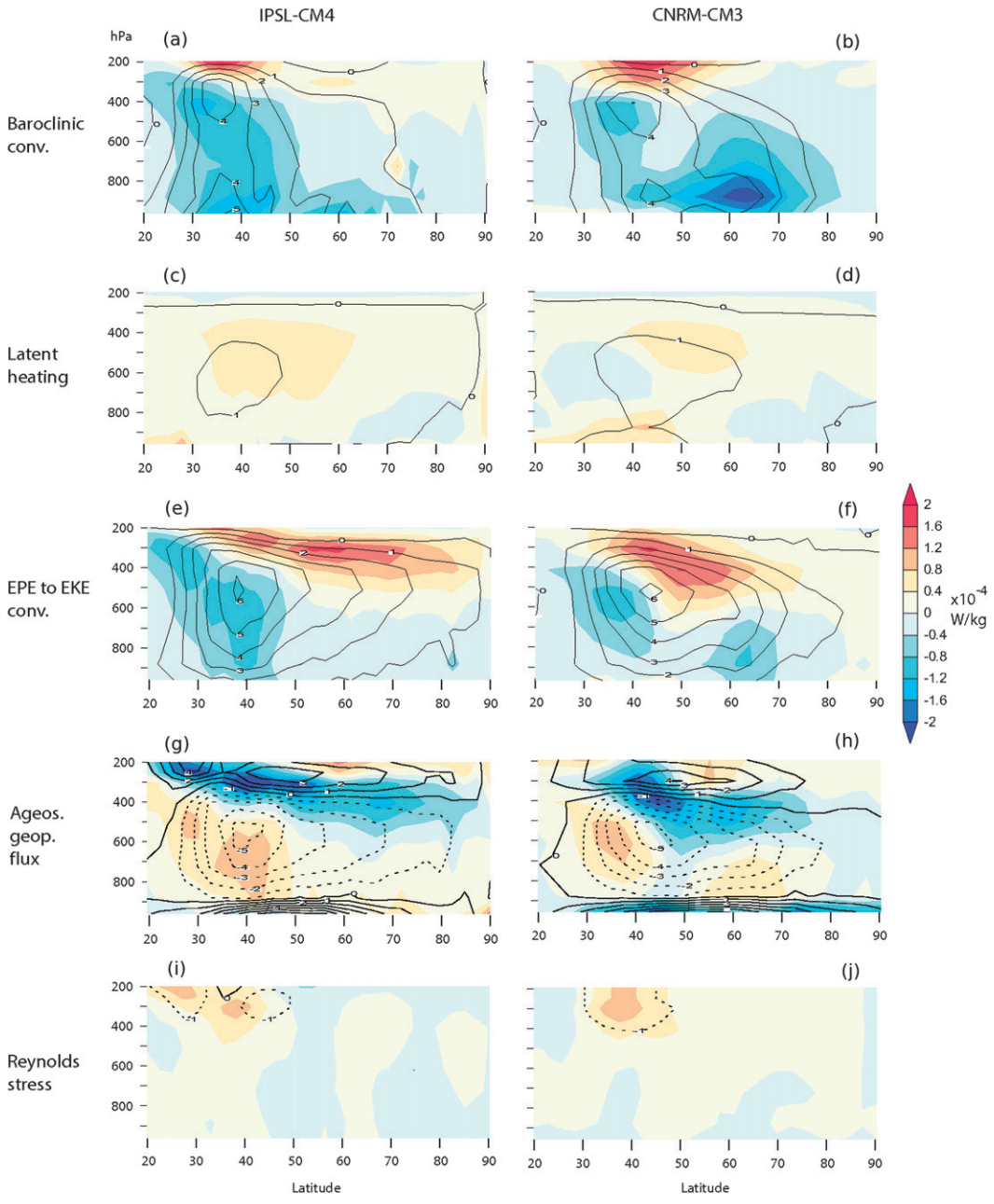

FIG. 9. Zonally averaged main DJF EPE and EKE generation terms, from 925 to 200 hPa and 20° to 90°N, for the (left) IPSL-CM4 model and the (right) CNRM-CM3 model. (a),(b) Baroclinic generation term; (c),(d) eddy latent heating term (not including the surface latent flux); (e),(f) EPE to EKE conversion term; (g),(h) EKE removal through ageostrophic geopotential flux; (i),(j) Reynolds stress. CTR simulations as isolines, contours every 10^{-4} W kg^{-1}. In color, (4CO2 − CTR) differences. Units in 10^{-4} W kg^{-1}.

changes correspond to a northeastward enhancement of the storm track.

In the western part of the basin (around 160°E), the synoptic activity changes are mostly due to a baroclinic reduction of the EPE generation, as in the IPSL model, by about 1.5 W m^{-2}, whereas the latent heating is only slightly reduced (Fig. 5b). Therefore, the relative role of the latent heat effects versus the baroclinic effects in the 4CO2 run is increased compared to that in CTR. The strong baroclinic loss in the western part of the North Pacific (between 135°E and 170°W) is primarily due to a strong reduction in the eddy heat flux magnitude and in the mean vertical stratification (Fig. 6b). An eddy heat flux reduction highlights a positive feedback,

in which eddy growth is reduced due to a reduction in the eddy activity, which of course relates to a reduced generation rate.

In the eastern part of the North Pacific, the reason for the northeastward displacement is not obvious but seems equally related to latent heat effects and to baroclinic effects in the generation terms (Figs. 7b and 7d).

3) VERTICAL STRUCTURE

As for the IPSL model, the negative differences in the baroclinic conversion in the CNRM model are located in the lower troposphere, whereas the positive differences are found in the uppermost part of the troposphere (not shown). One exception concerns the North Atlantic where the positive changes are found both in the upper and the lower parts of the atmosphere, the latter corresponding to the surface baroclinicity decrease (Fig. 3b).

The zonally averaged structure of the conversion terms (Fig. 9, right panels) is similar to the ones found for the IPSL model, both in terms of CTR values and differences. The physical explanation for the pattern of zonally averaged EKE changes (Fig. 2d) may be found in an upward shift of the baroclinic conversion, and an upward and poleward shift of the latent heating, with both resulting in an upward and poleward displacement of the EPE to EKE conversion, further relocated through ageostrophic geopotential fluxes.

6. Discussion and conclusions

Storm track dynamics are quite complex and understanding the processes governing their behavior under increased GHG concentrations is a delicate task, because of potentially compensating factors. Our aim is to consider the different possible patterns of behavior for Northern Hemisphere storm tracks. We concentrate on two models in order to develop a deeper understanding of the similarities and differences as well as the physical processes involved.

The latitudinal and vertical structures of the zonally averaged eddy kinetic energy changes are quite similar in the two models and are consistent with the IPCC-AR4 model-mean behavior considered in Yin (2005) for a GHG increase. They consist of poleward and upward shifts of the synoptic activity (Fig. 2). Nevertheless, the spatial patterns of the EKE changes in the Northern Hemisphere in the two models are in fact very different (Fig. 1). The IPSL-CM4 model suggests a strong decrease in North Atlantic synoptic activity, especially on the southern flank of the simulated preindustrial storm track. In the eastern North Pacific region, the synoptic activity is found to be displaced and enhanced eastward, close to the North American continent and also over it. In the CNRM-CM3 model, the simulated changes are different and sometimes opposite. Over the North Atlantic region, the synoptic activity is enhanced, corresponding to an eastward extension of the North Atlantic storm track. Over the North Pacific region, the synoptic activity is reduced to the north in the western part of the basin, whereas it is enhanced poleward in its eastern part. The questions arising from these differences in the simulations of the two models are whether they can be attributed to the same physical processes acting differently or directly to different processes. Considering the surface temperature changes can help explain part of storm track changes in the North Atlantic due to surface baroclinicity changes at the beginning of the storm tracks (Fig. 3). Nevertheless, this is not convincing for all regions, especially for the eastern part of the storm tracks. Also, we expect that the roles played by water vapor and latent heat release could be significantly changed for warmer climates.

To gain a clear view of the different processes involved in the simulated changes in the synoptic activity, we have examined the eddy energy equations. The different terms entering these equations allow for a clear quantification of the different processes involved in eddy energy generation or dissipation, through either purely dynamical or diabatic processes. First, we perform this analysis on NCEP–NCAR reanalyses and the CTR simulations of the two models (section 4, Fig. 4). This highlights the role played by baroclinic generation in the energetics of the transient eddies, followed by latent heating, which is of secondary importance in the first phase of developing storms, then equivalent. The local dissipation of eddy kinetic energy first occurs through ageostrophic geopotential advection processes, then through barotropic destruction (friction has not been considered but seems to be of an equal order of magnitude). Concerning the comparison between the NCEP–NCAR reanalyses and the CTR runs, no major discrepancies are found, except for a weak moist heating in the IPSL model. The conversion terms are well simulated for the North Atlantic region, while the dispersion is greater for the North Pacific region.

In the North Atlantic, the decrease in storm track activity simulated by the IPSL model is primarily due to baroclinic effects (Figs. 5 and 7), which are themselves caused by the reduced efficiency of the eddies to convert energy from the mean flow (Fig. 6). On the other hand, in the CNRM-CM3, the cause for the synoptic changes in the North Atlantic is to be found both in the baroclinic and latent heating processes, which are enhanced in the 4CO2 simulation in the second part of the

storm track (east of 45°W; Figs. 5 and 7). In the North Pacific, the weak synoptic decrease in the first part of the storm track is related to baroclinic changes in the IPSL model, which are also due to changes in eddy efficiency. Significant baroclinic changes occur in the western part of the North Pacific in the CNRM model but are predominantly due to a strong negative feedback in eddy growth. In the eastern part of the basin, diabatic and baroclinic changes are of the same order in each model. The strong latent heating differences simulated in the IPSL model in this area might be an amplification of the model bias. The upward and poleward shift of the zonally averaged EKE involves an upward enhancement of the baroclinic generation in the upper troposphere in both models, together with an upward and poleward displacement of the enhanced latent heating, which is further relocated by ageostrophic geopotential fluxes.

Latent heating differences are usually positive, consistent with moister conditions under warmer climates, except when synoptic changes are strongly negative (Figs. 1 and 7). We might think of latent heat release as an amplification factor of the baroclinic changes. Positive (negative) baroclinic differences at the beginning of the storm track result in stronger (weaker) synoptic activity, which implies more (less) energy being added to perturbations from latent processes as a direct consequence of the greater (weaker) number and/or intensity of perturbations. Nevertheless, there is an asymmetry in the amplification that stands for both models. When baroclinic differences are negative, the corresponding changes in latent heating are negative too, but of very small amplitude. When baroclinic differences are positive, the latent heat release changes are usually positive and as strong as the former. For a given synoptic activity, latent heat release will be stronger (weaker) in a warmer (colder) climate.

In conclusion, despite the general agreement of the coupled models to simulate broad-scale features of global warming—such as the polar amplification, a stronger temperature increase over the continents compared to the oceans, and an upward and poleward shift of the zonally averaged storm tracks—the response in terms of synoptic activity is complex and nonzonal. Despite their different patterns of behavior, the two models considered here show that the primary cause for synoptic activity changes are linked to baroclinic conversion changes, and in both models, latent effects react similarly, with a weak amplification of negative baroclinic differences and a strong amplification of the positive ones. Ageostrophic geopotential fluxes are also important to relocating the eddy energy generation changes, especially in the vertical. The greater amount of water contained in warmer air implies greater latent heat released for a given synoptic activity. Condensation and evaporation, which have been shown to be quite important in this study, are among the most difficult parameters to model. The very small scale at which these processes occur implies a need for parameterization in GCMs, which might not be appropriate for climates that are very different from the modern ones. Special attention should therefore be paid to this parameterization when considering the storm track behavior in nonmodern climates.

The primary role of the baroclinic generation term highlights the role of changes in temperature gradients in very specific regions on synoptic activity, especially at the beginning of the storm tracks, around the oceanic fronts separating the subtropical to the subpolar gyres on the western side of the oceanic basins. The displacement of the fronts and different temperature changes on each side of the fronts are important to consider. In particular, the Labrador and Greenland–Iceland–Norwegian (GIN) Seas are important regions to consider since oceanic convection takes place there and could be modified under GHG changes (Solomon et al. 2007). Nevertheless, this study also shows that the time-mean baroclinicity of the atmosphere is not the only parameter that influences the baroclinic generation term changes, and that other effects, like changes in the efficiency of the eddies to convert energy from the mean flow, can also be fundamental, as is the case in the IPSL model. The role played by the different components of the baroclinic generation term could be very model dependent, as suggested by the differences found between the two models studied here.

This study of two differently behaving models highlights the fundamental role played by baroclinic and latent heating generation terms, and by ageostrophic geopotential fluxes, in relocating these changes. It would hereafter be interesting to study these terms specifically when considering the responses of other IPCC-AR4 models, and especially for simulations of the twentieth century, which could be compared to the reanalyses. Also, it could be interesting to use similar diagnostics for considering climatological changes for other periods of years, when the relative roles of the different processes can be different.

Acknowledgments. We acknowledge the three reviewers, who strongly contributed to improving the coherence of the paper. Thanks also go to Gwendal Rivière, Laurent Terray, Paul Valdes, and Jean-François Royer for their bibliographical advice and comments on a draft of this paper. This work, performed within the framework of Etude des Scénarios Climatiques

Réalisés par l'IPSL et Météo-France (ESCRIME), has been supported by the European Commission Sixth Framework Program (ENSEMBLES Contract GOGE-CT-2003-505539) and by the ANR BLANC project Impact de Décharges d'Eau Douce Provenant de la Glace Continentale sur le Climat Européen et Méditerranéen (IDEGLACE; ANR-05-BLAN-310-01). NCEP–NCAR reanalysis data were provided by NOAA/OAR/ESRLPSD, Boulder, Colorado, from their Web site (http://www.cdc.noaa.gov).

REFERENCES

Baehr, C., B. Pouponneau, F. Ayrault, and A. Joly, 1999: Dynamical characterization of the FASTEX cyclogenesis cases. *Quart. J. Roy. Meteor. Soc.,* **125,** 3469–3494.

Bengtsson, L., K. I. Hodges, and E. Roeckner, 2006: Storm tracks and climate change. *J. Climate,* **19,** 3518–3543.

Black, R. X., 1998: The maintenance of extratropical intraseasonal transient eddy activity in the GEOS-1 assimilated dataset. *J. Atmos. Sci.,* **55,** 3159–3175.

——, and R. M. Dole, 2000: Storm tracks and barotropic deformation in climate models. *J. Climate,* **13,** 2712–2728.

Blackmon, M. L., 1976: A climatological spectral study of the 500 mb geopotential height of the Northern Hemisphere. *J. Atmos. Sci.,* **33,** 1607–1623.

Carlson, T. N., 1980: Airflow through midlatitude cyclones and the comma cloud pattern. *Mon. Wea. Rev.,* **108,** 1498–1509.

Chang, E. K. M., and I. Orlanski, 1993: On the dynamics of a storm track. *J. Atmos. Sci.,* **50,** 999–1015.

——, and P. Zurita-Gotor, 2007: Simulating the seasonal cycle of the Northern Hemisphere storm tracks using idealized nonlinear storm-track models. *J. Atmos. Sci.,* **64,** 2309–2331.

——, S. Lee, and K. L. Swanson, 2002: Storm track dynamics. *J. Climate,* **15,** 2163–2183.

Fyfe, J. C., 2003: Extratropical Southern Hemisphere cyclones: Harbingers of climate change? *J. Climate,* **16,** 2802–2805.

Geng, Q. Z., and M. Sugi, 2003: Possible change of extratropical cyclone activity due to enhanced greenhouse gases and sulfate aerosols—Study with a high-resolution AGCM. *J. Climate,* **16,** 2262–2274.

Hall, N. M. J., B. J. Hoskins, P. Valdes, and C. A. Senior, 1994: Storm track in a high-resolution GCM with doubled carbon dioxide. *Quart. J. Roy. Meteor. Soc.,* **120,** 1209–1230.

Hoskins, B. J., and F. P. Bretherton, 1972: Atmospheric frontogenesis models: Mathematical formulation and solution. *J. Atmos. Sci.,* **29,** 11–37.

——, and P. J. Valdes, 1990: On the existence of storm tracks. *J. Atmos. Sci.,* **47,** 1854–1864.

——, and K. I. Hodges, 2002: New perspectives on the Northern Hemisphere winter storm tracks. *J. Atmos. Sci.,* **59,** 1041–1061.

——, H. H. Hsu, I. N. James, M. Masutani, P. D. Sardeshmukh, and G. H. White, 1989: Diagnostics of the global atmospheric circulation based on ECMWF analyses 1979–1989. WRCP Tech. Rep. 27, 217 pp.

Jung, T., S. K. Gulev, I. Rudeva, and V. Soloviov, 2006: Sensitivity of extratropical cyclone characteristics to horizontal resolution in the ECMWF model. *Quart. J. Roy. Meteor. Soc.,* **132,** 1839–1857.

Kageyama, M., P. J. Valdes, G. Ramstein, C. Hewitt, and U. Wyputta, 1999: Northern Hemisphere storm tracks in present day and Last Glacial Maximum climate simulations: A comparison of the European PMIP models. *J. Climate,* **12,** 742–760.

Lackmann, G. M., D. Keyser, and L. E. Bosart, 1999: Energetics of an intensifying jet streak during the Experiment on Rapidly Intensifying Cyclones over the Atlantic (ERICA). *Mon. Wea. Rev.,* **127,** 2777–2795.

Lambert, S., and J. C. Fyfe, 2006: Changes in winter cyclone frequencies and strengths simulated in enhanced greenhouse gas experiments: Results from the models participating in the IPCC diagnostic exercise. *Climate Dyn.,* **26,** 713–728.

Marti, O., and Coauthors, 2006: The new IPSL climate system model: IPSL-CM4. Note du Pôle de Modélisation 26, Institut Pierre Simon Laplace, Jussieu, France. [Available online at http://dods.ipsl.jussieu.fr/omamce/IPSLCM4/DocIPSLCM4/HTML/.]

Masson-Delmotte, V., and Coauthors, 2005: Past and future polar amplification of climate change: Climate model intercomparisons and ice-core constraints. *Climate Dyn.,* **26,** 513–529, doi:10.1007/s00382-005-0081-9.

McCabe, G. J., M. P. Clark, and M. C. Serreze, 2001: Trends in Northern Hemisphere surface cyclone frequency and intensity. *J. Climate,* **14,** 2763–2768.

Moritz, R. E., C. M. Bitz, and E. J. Steig, 2002: Dynamics of recent climate change in the Arctic. *Science,* **297,** 1497–1502.

Orlanski, I., 2003: Bifurcation in eddy life cycles: Implications for storm track variability. *J. Atmos. Sci.,* **60,** 993–1023.

——, and J. Katzfey, 1991: The life cycle of a cyclone in the Southern Hemisphere. Part I: Eddy energy budget. *J. Atmos. Sci.,* **48,** 1972–1998.

——, and J. Sheldon, 1995: Stages in the energetics of baroclinic systems. *Tellus,* **47A,** 605–628.

Peixoto, J., and A. H. Oort, 1992: *Physics of Climate.* American Institute of Physics, 520 pp.

Rivière, G., and A. Joly, 2006a: Role of the low-frequency deformation field on the explosive growth of extratropical cyclones at the jet exit. Part I: Barotropic critical region. *J. Atmos. Sci.,* **63,** 1965–1981.

——, and ——, 2006b: Role of the low-frequency deformation field on the explosive growth of extratropical cyclones at the jet exit. Part II: Baroclinic critical region. *J. Atmos. Sci.,* **63,** 1982–1995.

——, and I. Orlanski, 2007: Characteristics of the Atlantic storm-track eddy activity and its relation with the North Atlantic Oscillation. *J. Atmos. Sci.,* **64,** 241–266.

Salas-Mélia, D., and Coauthors, 2005: Description and validation of the CNRM-CM3 global coupled model. CNRM Working Note 103.

Solomon, S., and Coeditors, 2007: *Climate Change 2007: The Physical Science Basis.* Cambridge University Press, 996 pp.

Sutton, R. T., B. Dong, and J. M. Gregory, 2007: Land/sea warming ratio in response to climate change: IPCC AR4 model results and comparison with observations. *Geophys. Res. Lett.,* **34,** L02701, doi:10.1029/2006GL028164.

Wallace, J. M., G.-H. Lim, and M. L. Blackmon, 1988: Relationship between cyclone tracks, anticyclone tracks and baroclinic waveguides. *J. Atmos. Sci.,* **45,** 439–463.

Yin, J. H., 2005: A consistent poleward shift of the storm tracks in simulations of 21st century climate. *Geophys. Res. Lett.,* **32,** L18701, doi:10.1029/2005GL023684.